JOURNAL OF SOLID STATE CHEMISTRY 102, 106–114 (1993)

Crystal Structure and Electrical Properties of the Pyrochlore Ruthenate $Bi_{2-x}Y_xRu_2O_7$

R. KANNO,* Y. TAKEDA,† T. YAMAMOTO,†‡ Y. KAWAMOTO, AND O. YAMAMOTO†

Department of Chemistry, Faculty of Science, Kobe University, Kobe 657, and †Department of Chemistry, Faculty of Engineering, Mie University, Tsu, 514 Japan

Received September 24, 1991; in revised form June 18, 1992; accepted June 24, 1992

The bismuth yttrium pyrochlore ruthenates $Bi_{2-x}Y_xRu_2O_7$ have been synthesized and characterized by X-ray Rietveld structure refinement and electrical conductivity measurement. Room temperature resistivities increase with x, and a change from metallic to semiconducting behavior is observed between $x = 1.2$ and 1.4. The distortion of the RuO_6 octahedra and the bend in the RuO_6 zig-zag chains increase with x. The transition from metallic to semiconducting state is correlated with the variation of the Ru–O–Ru angle from 139° at $x = 0.0$ to 129° at $x = 2.0$. The Ru–O bond length in the RuO_6 octahedra increases in the interval $0 \le x \le 1.2$. This variation is understood to result from the contribution of Bi orbitals to the conduction band; in the metallic regime, $0 \le x \le 1.2$, the electron transfer leads to short Ru–O bond length, whereas in the nonmetallic state there is little Ru–O bond length variation because there is no contribution of the Bi electrons to the Ru 4*d* state.

Introduction

The pyrochlore ruthenates are technologically important materials as catalysts (*1*), electrocatalysts (*2*), and conducting components in thick-film resistors (*3–5*). Their electronic properties are of intrinsic interest, since the Ru : 4*d* electrons are on the borderline between localized and itinerant behavior. For example, the bismuth ruthenate $Bi_2Ru_2O_7$ and the lead ruthenate $Pb_2Ru_2O_{6.5}$ are metallic Pauli paramagnets with a nearly temperature-independent resistivity, whereas the rare-earth ruthenates $Ln_2Ru_2O_7$ (*Ln* = Pr–Lu) and $Y_2Ru_2O_7$ are all semiconductors with a spontaneous ruthenium atomic moment (*6–8*). The electronic structure of the pyrochlore has recently been studied for the quaternary ruthenate $Bi_{2-x}Gd_xRu_2O_7$, which exhibited an almost continuous range of compositions between $x = 0$ and $x = 2.0$. Based on ultraviolet He(I) photoelectron spectroscopy (XPS, UPS, and EELS measurements), the metallic behavior of bismuth and lead ruthenates is attributed to significant mixing between the Ru 4*d* band and the 6*s* band of Bi and Pb (*9*). More recently, the band structures of $Pb_2Ru_2O_{6.5}$ and $Bi_2Ru_2O_7$ have been calculated using the pseudofunction method (*10*). According to this investigation, the 6*s* states of Pb or Bi are very deep and unlikely to be mixed with the Ru 4*d*

* To whom correspondence should be addressed.

‡ Present address: ISIR, Osaka University, Ibaragi 567, Japan.

0022-4596/93 $5.00

states at the Fermi surface, and the unoccupied Pb or Bi 6*p* states are significantly closer to E_F and contribute to their metallic conductivity by mixing with the Ru 4*d* state via the framework oxygen. Shifts from metallic to semiconducting behavior as a function of composition were also observed for the $A_2(Ru_{2-x}A_x)O_{7-y}$ (A = Pb or Bi) system (*11*).

While the conduction mechanisms of the ternary and quaternary ruthenate pyrochlores have been extensively studied, the relationship between their electronic and crystal structures is poorly understood. Like the cubic-perovskite structure, the pyrochlores $A_2B_2O_6O'$ have a BO_3 array of corner-shared octahedra, but the *B*–O–*B* angles are reduced from 180° to about 130° (*7, 12, 13*). Reduction of the *B*–O–*B* angles from 180° reduces the *B*–O–*B* overlap integrals; the electrical properties of the pyrochlores might thus be affected by a small change in the *B*–O–*B* angle. Previous structural studies on $Bi_2Ru_2O_7$ (*14, 15*) and two $Ln_2Ru_2O_7$ (Ln = Nd, Lu) pyrochlores (*15*) showed that the Ru–O bond distances are 2.0 ± 0.1 Å in all cases and that the Ru–O–Ru bond angles are all about 130°, leading to the idea that the Ru–O bond distances or the Ru–O–Ru bond angles do not play a significant role in constructing the electronic structure (*16*). Therefore, a systematic study of the structure determination for the ruthenate pyrochlores with the metallic semiconducting system has yet to be carried out. The quaternary pyrochlore ruthenates, the end members of which are respectively a metal and an insulator, might thus afford the possibility of studying changes in crystal and electronic structures accompanying a metal-to-nonmetal transition; we report here the first systematic structural analysis of the pyrochlore ruthenates $Bi_{2-x}Y_xRu_2O_7$ using X-ray Rietveld method together with an investigation of the electrical properties of the solid solution.

Experimental

The ternary oxides $A_2Ru_2O_7$ (A = Bi, Y) and the quarternary oxides $Bi_{2-x}Y_xRu_2O_7$ were prepared by heating an appropriate molar ratios of RuO_2, Bi_2O_3, and Y_2O_3 (RuO_2: Furuuchi Chemicals, Ltd., >99.99% purity; Bi_2O_3: Nakarai Chemicals. Ltd., >99.9% purity; Y_2O_3: Nakarai Chemicals. Ltd., >99.99% purity). The starting materials were dried for 2 days in air at 1000°C for Y_2O_3 and at 500°C for RuO_2 Bi_2O_3. They were weighed, mixed, pelletized in a nitrogen-filled glove box, and put into a platinum tube to avoid a reaction between the silica tube and the sample. The platinum tube was then sealed in an evacuated silica tube and heated at 500°C for 12 hr and at 900–1200°C for 30 to 40 hr with regrinding between successive firings. The loss of ruthenium was thus minimized by the above reaction procedure.

X-Ray diffraction (XRD) patterns of the powdered samples were obtained using a high-power XR diffractometer (Rigaku RAD 12kW) with monochromated Cu$K\alpha$ radiation and a scintillation detector. The lattice parameters were refined by Rietveld analysis using the computer program RIETAN provided by Izumi (*17*). Reflection positions and intensities were calculated for both Cu$K\alpha_1$ and Cu$K\alpha_2$, with a factor of 0.5 applied to the latter's calculated integrated intensities. A pseudo-Voigt profile function was used; the mixing parameter γ was included in the least-squares refinement.

The electrical resistivity was measured with sintered materials with dimensions of approximately 2 × 2 × 10 mm. The data were obtained by a dc four-probe method in the temperature range $15 \leq T \leq 300$ K using a CHINO US-36 electrical conductivity measurement system. The temperature was monitored with a calibrated carbon-glass thermometer mounted near the sample.

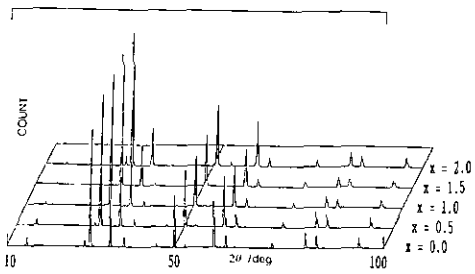

FIG. 1. X-Ray diffraction patterns for $Bi_{2-x}Y_xRu_2O_7$.

Results and Discussion

Synthesis

Monophasic properties of the pyrochlore structure were obtained for the quaternary ruthenates, $Bi_{2-x}Y_xRu_2O_7$, for the whole range of solid solution; the firing temperature required to produce a single-phase material increased from 900 to 1200°C with increasing yttrium content. Figures 1 and 2 show the X-ray diffraction patterns and composition dependence of the lattice parameters, after Rietveld refinement, for $Bi_{2-x}Y_xRu_2O_7$ ($0 \leq x \leq 2.0$), respectively. The lattice parameters decrease with x, and a gradual slope change is observed at $1.0 \leq x \leq 2.0$. The narrow two-phase region of $1.5 < x < 1.6$ reported for the $Bi_{2-x}Gd_xRu_2O_7$ system (*9*) was not observed. There were no extra XRD peaks due to a superstructure caused by vacancy ordering which is found in $Pb_2Ru_2O_{6.5}$ (*18*).

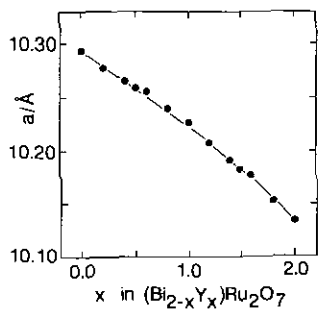

FIG. 2. Composition dependence of lattice parameters for $Bi_{2-x}Y_xRu_2O_7$.

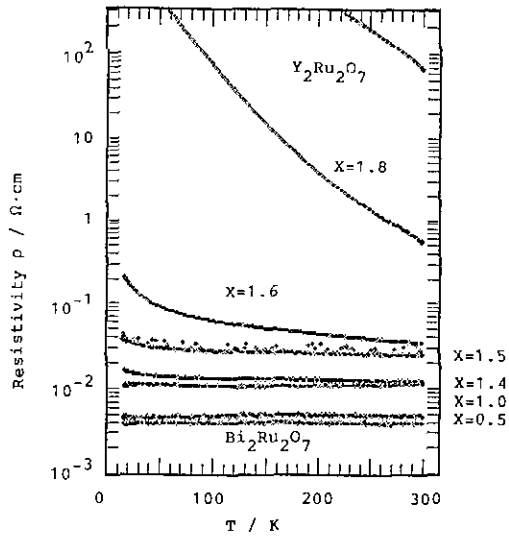

FIG. 3. Temperature dependence of resistivity for $Bi_{2-x}Y_xRu_2O_7$.

Electrical Properties

Electrical resistivity data for the system $Bi_{2-x}Y_xRu_2O_7$ are given in Fig. 3. The data show that $Bi_2Ru_2O_7$ has metallic properties with a low and nearly temperature-independent resistivity of $\rho = 4 \times 10^{-3}\ \Omega \cdot$ cm, while in $Y_2Ru_2O_7$, the semiconducting properties were observed with a room temperature resistivity of $\rho = 10^2\ \Omega \cdot$ cm. In the quaternary system, $Bi_{2-x}Y_xRu_2O_7$, the resistivity increases with x and a change from metallic to semiconducting behavior is observed between $x = 1.2$ and 1.4. In the previous studies on $Bi_{2-x}Gd_xRu_2O_7$, a metal–nonmetal transition was observed at $x \approx 1.5$, which is slightly different from the above data.

Crystal Structure

Refinement of the structure proceeded with space group *Fd3m*. Initial coordinates

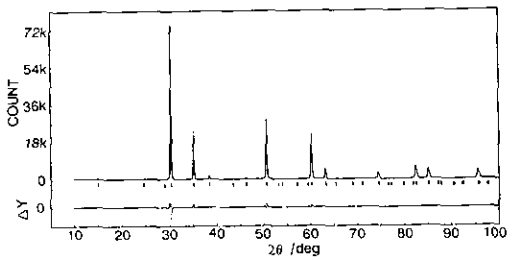

FIG. 4. Observed, calculated, and difference plots of $BiYRu_2O_7$ ($x = 1.0$ in $Bi_{2-x}Y_xRu_2O_7$).

were taken as follows: Bi(Y), 16*d* ($\frac{5}{8}$, $\frac{5}{8}$, $\frac{5}{8}$); Ru, 16*c* ($\frac{1}{8}$, $\frac{1}{8}$, $\frac{1}{8}$); O(1), 48*f* (x, 0, 0), $x \approx 0.2$; O(2), 8*b* ($\frac{1}{2}$, $\frac{1}{2}$, $\frac{1}{2}$). The refinement was done in stages, with the atomic coordinates and thermal parameters held fixed in the initial calculations and subsequently allowed to vary only after the scale, background, half-width, and unit-cell parameters were close to convergence to their optimum values. The site occupation parameters for Bi/Y atoms on the 16*d* sites were fixed at the value of the starting compositions. During the later refinements, when temperature factors were refined, the B_{eq}'s for the O(1) and O(2) sites had to be constrained to the same value; otherwise the refinement was unstable. In the final refinement, a total of 19 positional, thermal, and instrumental parameters were refined. The results for the $Bi_{2-x}Y_xRu_2O_7$ system are summarized in Table I. For definition of R factors, see Ref. (*17*). Figure 4 shows observed, calculated, and difference plots for $BiYRu_2O_7$ ($x = 1.0$ in $Bi_{2-x}Y_xRu_2O_7$). Table II lists the interatomic distances and bond angles.

Figures 5 and 6 show, respectively, composition dependence of the interatomic distances and angles in the $Bi_{2-x}Y_xRu_2O_7$ system. The most interesting features of these figures are the Ru–O(1) variations. The Bi(Y)–O(1) and Bi(Y)–O(2) bond lengths decrease with increasing x throughout the whole composition range, whereas the Ru–O(1) bond length increases with x in the interval $0 \leq x \leq 1.2$, varying little with x in the interval $1.2 \leq x \leq 2.0$. The decrease in the lattice parameters and Bi(Y)–O(1) and Bi(Y)–O(2) bond lengths with x is explained by the substitution of Bi^{3+} (1.11-Å) ions into smaller Y^{3+} (1.02-Å) ions. However, the increase in the Ru–O(1) bond length is inconsistent with the change expected from the lattice parameter variation.

The Ru–O(1)–Ru angle shown in Fig. 6 decreases with x from 139° at $x = 0.0$ to 129° at $x = 2.0$. The O(1)–Ru–O(1) angles vary with x from 88.8° and 91.2° at $x = 0.0$ to 81.8° and 98.2° at $x = 2.0$, respectively, indicating a considerable increase in the distortion of RuO_6 octahedra. The pyrochlore structure consists of a framework of corner-sharing RuO_6 octahedra that are linked into zig-zag chains. Each O atom is fourfold coordinated to two Ru atoms and two Bi atoms (see Fig. 7). The arrow in Fig. 7 shows the shift of the O(1) position with the substitution of Bi^{3+} ions into Y^{3+} ions. The O(1) atom shifts away from its Ru nearest neighbor toward its A (Bi or Y) nearest neighbor since Y^{3+} ions are much smaller than Bi^{3+} ions.

The structure refinement results are summarized as follows. With increasing Y^{3+} content, (i) the Ru–O bond length in the RuO_6 octahedra increases in the interval $0 \leq x \leq 1.2$, (ii) the distortion of the RuO_6 octahedra increases in the interval $0 \leq x \leq 2.0$, and (iii) the bend in the RuO_6 zig-zag chains increases in the interval $0 \leq x \leq 2.0$. The above structural changes reduce Ru–O–Ru interaction with increasing x.

In the previous studies, the electrical properties of the ruthenate pyrochlore are understood as follows. For both $Y_2Ru_2O_7$ and rare earth ruthenates, the relatively unfavorable Ru–O–Ru angle coupled with competition for the 0:2*p* orbitals by the acidic A^{3+} ions yields a t_{2g} band insufficiently wide to sustain itinerant behavior (*9*). The band structure calculation also con-

TABLE I

RIETVELD REFINEMENT RESULTS FOR $Bi_{2-x}Y_xRu_2O_7$

	$x = 0.0^a$	$x = 0.2$	$x = 0.4$	$x = 0.5$	$x = 0.6$
Lattice constant, a(Å)	10.2934(1)	10.2775(1)	10.2654(1)	10.2592(1)	10.2565(1)
Cell volume (Å^3)	1090.62(1)	1085.58(1)	1081.75(1)	1079.79(1)	1078.94(1)
x parameter	0.190(5)	0.193(4)	0.196(3)	0.199(4)	0.197(4)
$x * a$ (Å)	1.98(6)	1.99(5)	2.01(4)	2.04(5)	2.03(4)
B_{eq}(Bi/Y) (Å^2)	0.9(2)	0.8(2)	0.8(2)	0.1(2)	0.8(2)
B_{eq}(Ru) (Å^2)	0.1	0.8(2)	0.1(2)	0.1(2)	0.1(2)
B_{eq}(O) (Å^2)	0.5(17)	2.0(16)	0.7(1)	0.9(1)	0.6(1)
R_{WP}	12.58	14.23	10.95	13.77	13.23
R_P	8.96	10.51	7.82	10.12	9.52
R_E	3.59	3.55	3.57	3.63	3.64
R_I	1.94	5.64	3.43	4.93	4.07
R_F	3.27	8.14	5.20	6.98	5.34
	$x = 0.8$	$x = 1.0$		$x = 1.2$	$x = 1.4$
Lattice constant, a(Å)	10.2404(1)	10.2273(1)		10.2080(1)	10.1924(11)
Cell volume (Å^3)	1073.87(1)	1069.75(1)		1063.71(1)	1058.84(1)
x parameter	0.200(2)	0.204(2)		0.204(3)	0.203(2)
$x * a$ (Å)	2.05(3)	2.09(2)		2.09(3)	2.08(3)
B_{eq}(Bi/Y) (Å^2)	0.6(1)	0.5(1)		0.3(2)	0.1(2)
B_{eq}(Ru) (Å^2)	0.1(2)	0.2(2)		0.1(2)	0.4(2)
B_{eq}(O) (Å^2)	0.4(8)	0.9(7)		0.4(8)	0.4(7)
R_{WP}	9.28	8.06		9.48	9.15
R_P	6.71	5.57		6.81	6.66
R_E	3.72	3.62		3.74	3.63
R_I	3.06	2.31		2.70	2.64
R_F	4.71	2.86		4.64	4.19
	$x = 1.5$	$x = 1.6$		$x = 1.8$	$x = 2.0$
Lattice constant, a(Å)	10.1834(11)	10.1774(11)		10.1525(1)	10.1342(2)
Cell volume (Å^3)	1056.04(1)	1054.17(1)		1046.45(1)	1040.80(1)
x parameter	0.206(2)	0.206(2)		0.207(2)	0.208(4)
$x * a$ (Å)	2.11(3)	2.10(1)		2.11(3)	2.11(4)
B_{eq}(Bi/Y) (Å^2)	0.3(2)	0.4(3)		0.1(1)	0.2(2)
B_{eq}(Ru) (Å^2)	0.1(2)	0.1(2)		0.1(1)	0.3(1)
B_{eq}(O) (Å^2)	0.2(6)	0.2(7)		0.1(6)	0.3(1)
R_{WP}	8.65	8.91		12.00	19.56
R_P	6.01	6.60		8.50	13.18
R_E	3.67	3.60		3.73	3.74
R_I	2.45	1.99		2.49	4.10
R_F	4.28	2.46		3.02	5.53

[a] Composition (x in $Bi_{2-x}Y_xRu_2O_7$)

firmed that $Y_2Ru_2O_7$ has a narrow t_{2g} band at E_F and is therefore a Mott insulator (*10*). By contrast in $Bi_2Ru_2O_7$ where the Bi^{3+} ions have a $6s^2$ valence-electron configuration, Bi–O–Ru interactions appear to enhance the width of the Ru : $4d(t_{2g})$ band sufficiently to allow for metallic behavior and Pauli paramagnetism (*9*). The band structure calculation showed that the unoccupied Bi $6p$ states are significantly closer to E_F and con-

TABLE II

CALCULATED BOND DISTANCES (Å) AND ANGLES (deg) FOR $Bi_{2-x}Y_xRu_2O_7$

		$x = 0.0$	$x = 0.2$	$x = 0.4$	$x = 0.5$	$x = 0.6$
		Environment at A (A = Bi or Y) (16d)				
A–O1	×6	2.63(4)	2.60(3)	2.58(2)	2.54(3)	2.56(2)
A–O2	×2	2.22859(1)	2.22514(1)	2.22252(1)	2.22118(1)	2.22060(1)
O1–A–O1	×6	62.1(3)	62.4(2)	62.6(2)	62.8(3)	62.7(2)
	×6	117.8(3)	117.5(2)	117.3(2)	117.1(3)	117.2(2)
		Environment at ruthenium: Ru (16c)				
Ru–O1	×6	1.94(2)	1.949(17)	1.956(13)	1.966(19)	1.961(16)
O1–Ru–O1	×6	91.2(19)	92.5(13)	93.4(9)	94.5(12)	94.0(11)
	×6	88.8(19)	87.5(13)	86.6(9)	86.0(12)	86.0(11)
		Environment at oxygen: O1 (48f)				
Ru–O1–Ru	×1	139(3)	137(2)	136(2)	134(2)	135(2)
A–O1–A	×1	87(2)	88.6(15)	89.3(11)	90.3(16)	89.9(13)
A–O1–Ru	×4	104.5(10)	105.0(7)	105.3(5)	105.8(6)	105.6(5)
		$x = 0.8$	$x = 1.0$	$x = 1.2$		$x = 1.4$
		Environment at A (A = Bi or Y) (16d)				
A–O1	×6	2.544(19)	2.51(2)	2.50(2)		2.50(2)
A–O2	×2	2.21711(1)	2.21428(2)	2.21010(1)		2.20672(1)
O1–A–O1	×6	63.00(18)	63.3(2)	63.4(2)		63.3(2)
	×6	117.00(18)	116.6(2)	116.5(2)		116.6(2)
		Environment at ruthenium: Ru (16c)				
Ru–O1	×6	1.968(10)	1.981(15)	1.979(13)		1.943(12)
O1–Ru–O1	×6	95.0(7)	96.4(9)	96.5(8)		96.3(7)
	×6	85.0(7)	83.6(9)	83.5(8)		83.7(7)
		Environment at oxygen: O1 (48f)				
Ru–O1–Ru	×1	133.8(14)	131(2)	131.6(17)		131.9(15)
A–O1–A	×1	90.7(9)	92.0(12)	92.1(11)		91.9(9)
A–O1–Ru	×4	106.0(3)	106.5(4)	106.5(4)		106.4(3)
		$x = 1.5$	$x = 1.6$	$x = 1.8$		$x = 2.0$
		Environment at A (A = Bi or Y) (16d)				
A–O1	×6	2.485(18)	2.48(2)	2.470(19)		2.45(2)
A–O2	×2	2.20477(1)	2.20347(1)	2.19808(1)		2.19514(1)
O1–A–O1	×6	63.6(2)	63.5(2)	63.7(2)		63.9(3)
	×6	116.3(2)	116.4(2)	116.2(2)		116.0(3)
		Environment at ruthenium: Ru (16c)				
Ru–O1	×6	1.984(11)	1.980(12)	1.982(12)		1.986(16)
O1–Ru–O1	×6	97.3(6)	97.1(7)	97.6(7)		98.2(9)
	×6	82.7(6)	82.9(7)	82.4(7)		81.8(9)
		Environment at oxygen: O1 (48f)				
Ru–O1–Ru	×1	130.3(14)	130.7(15)	129.8(14)		129(2)
A–O1–A	×1	92.9(9)	92.6(9)	93.2(9)		93.7(13)
A–O1–Ru	×4	106.8(3)	106.4(3)	106.9(3)		107.1(4)

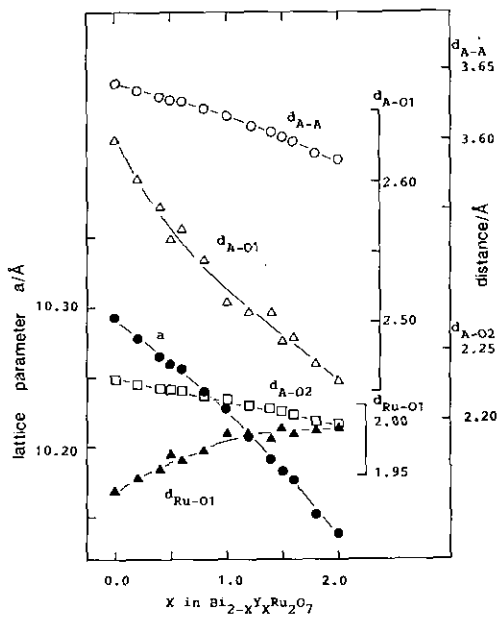

FIG. 5. Variation of the bond lengths in $Bi_{2-x}Y_xRu_2O_7$.

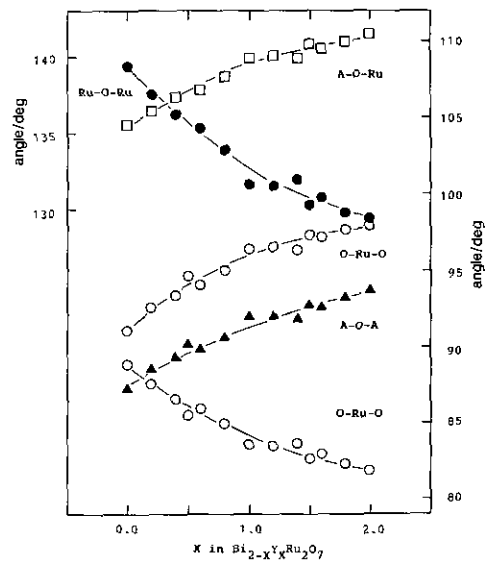

FIG. 6. Variation of the bond angles in $Bi_{2-x}Y_xRu_2O_7$.

tribute to their metallic conductivity by mixing with the Ru 4*d* state via the framework oxygen (*10*). The transition from nonmetallic to metallic behavior as *Ln* (*Ln* = rare earth) or Y ions are replaced by Bi ions introduces the idea that upper and lower Hubbard bands are separated by a well-defined energy gap in the nonmetallic regime. As the transfer integral that characterizes the width of the one-electron t_{2g} band increases with Bi content, the Hubbard bands broaden and eventually coalesce with a sudden jump from zero in the density of electronic states at the Fermi energy (*9*).

The transition from nonmetallic to metallic behavior in $Bi_{2-x}Y_xRu_2O_7$ is closely correlated with the structural variations. The substitution of Y^{3+} for Bi^{3+} introduces distortion in the RuO_6 octahedra; it also increases the bend in the RuO_6 zig-zag chains. The reduction of the O(1)–Ru–O(1) angle from 139° to 129° and the distortion of RuO_6 octahedra reduce the Ru–O(1) overlap integrals; this directly affects the electrical properties, leading to the transition from metallic to semiconducting state between $x = 1.2$ and 1.4. A smaller covalent energy was suggested by reducing the B–O–B angle from 180° (*19*), and is consistent with the above results on the $Bi_{2-x}Y_xRu_2O_7$ system.

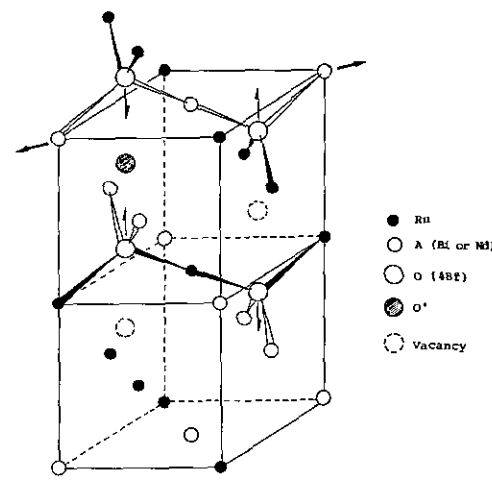

FIG. 7. Structure of $Bi_{2-x}Y_xRu_2O_7$.

As interesting is the relative position of the O(1) atom, with increasing x, it shifts away from its Ru nearest neighbor toward its A (Bi or Y) nearest neighbor in the compositional interval $0 \leq x \leq 1.0$ where the resistivity remains metallic behavior; this shift stops for $1.5 \leq x$ where the room temperature conduction is semiconducting. As a result of the oxygen shifts, the Ru–O(1) bond length increases with x in the interval $0 \leq x \leq 1.2$, varying little with x in the interval $1.2 \leq x \leq 2.0$. This bond length variation is attributed to the covalent admixture via Bi–O(1)–Ru. In the metallic regime the electron transfer from the Bi to Ru $4d$ state leads to shorter Ru–O(1) bond length; the contribution of the Bi orbitals to the Ru $4d$ state decreases as Bi^{3+} ions are replaced by Y^{3+} ions, leading to an increase in the Ru–O(1) bond length. In the nonmetallic state there is little Ru–O bond length variation because there is no contribution of the Bi orbitals to the conduction band.

It has become apparent that the electrical properties of the ruthenate pyrochlore depend on the structural variations. The same structural change in zig-zag BO_6 octahedra chains has been observed for the rare earth–titanium(III) perovskites, $LnTiO_3$ (Ln = rare earth), which form an isostructural series for Ln = La to Tm, including Y with the $GdFeO_3$-type structure (*20*). This type of structure is derived from the cubic perovskite cell by a cooperative set of twists of the TiO_6 octahedra, like the pyrochlore structure. Discontinuous changes in electrical and magnetic properties occur as the radius of Ln decreases: for Ln = La and Ce, metallic conductivity is observed with the metal–semiconductor transition at low temperatures; all other Ln are semiconducting. The single-crystal structural analysis showed that the Ti–O–Ti angle varies from 157° to 142° from La to Y, and the above changes in electrical properties are correlated with the variation of the Ti–O–Ti angle. These results on the pyrochlore and $GdFeO_3$-type structures indicate that the B–O–B angle variations highly affect the electrical properties in these systems, and that the structural studies are useful in clarifying the electrical property changes.

Conclusion

We synthesized the $Bi_{2-x}Y_xRu_2O_7$ solid solution with the pyrochlore structure. The resistivity increases with x and a change from metallic to semiconducting behavior is observed between 1.2 and 1.4. Structure analysis indicated that (i) the Ru–O bond length in the RuO_6 bond length in the RuO_6 octahedra increases, (ii) the distortion of the RuO_6 octahedra increases, and (iii) the bend in the RuO_6 zig-zag chains increases with increasing Y^{3+} contents. The Ru–O(1)–Ru angle variations might affect the Ru–O overlap integrals, leading to the transition from metallic to semiconducting state. The Ru–O(1) bond length variation can also be understood to result from the contribution of Bi orbitals to the conduction band; in the metallic regime the electron transfer leads to shorter Ru–O(1) bond length, whereas in the nonmetallic state there is little Ru–O bond length variation because there is no contribution of the Bi electrons to the Ru $4d$ state.

Acknowledgments

We thank Professor A. W. Sleight for reading the manuscript critically and Dr. F. Izumi of NIRIM for providing the computer program RIETAN. All computations for structure determination were carried out at the Mie University Information Processing Center. We gratefully acknowledge the support from Tokuyama Science Foundation. This work was supported partly by a Grant-in-Aid for Scientific Research on Chemistry of New Super Conductors from the Ministry of Education, Science and Culture.

References

1. A. T. Ashcroft, A. K. Cheetham, J. S. Foord, M. L. H. Green, C. P. Grey, A. J. Murrell, and P. D. F. Vernon, *Nature* **344,** 319 (1990).

2. R. G. EGDELL, J. B. GOODENOUGH, A. HAMNETT, AND C. C. NAISH, *J. Chem. Soc. Faraday Trans. 1* **79,** 893 (1983).
3. G. E. PIKE AND C. H. SEAGER, *J. Appl. Phys.* **48,** 5152 (1977).
4. P. F. CARCIA, A. FERRETI, AND A. SUNA, *J. Appl. Phys.* **53,** 5282 (1982).
5. N. SINNADURAI AND K. J. WILSON, *IEEE Trans. Components Hybrids Manuf. Technol.* **CHMT-5,** 308 (1982).
6. R. J. BOUCHARD AND J. L. GILLSON, *Mater. Res. Bull.* **6,** 669 (1971).
7. J. M. LONGO, P. M. RACCAH, AND J. B. GOODENOUGH, *Mater. Res. Bull.* **4,** 191 (1969).
8. R. ALEONARD, A. F. BERTHAND, M. C. MONTMORY, AND R. PAUTHENET, *J. Appl. Phys.* **33,** 1205 (1962).
9. P. A. COX, J. B. GOODENOUGH, P. J. TAVENER, D. TELLES, AND R. G. EGDELL, *J. Solid State Chem.* **62,** 360 (1986).
10. W. Y. HSU, R. V. KASOWSKI, T. MILLER, AND T.-C. CHIANG, *Appl. Phys. Lett.* **52,** 7 (1988).
11. R. A. BEYERLEIN, H. S. HOROWITZ, AND J. M. LONGO, *J. Solid State Chem.* **72,** 2 (1988).
12. A. W. SLEIGHT, *Inorg. Chem.* **7,** 1704 (1968).
13. M. A. SUBRAMANIAN, G. ARAVAMDAN, AND G. V. SUBBA RAO, *Prog. Solid State Chem.* **55,** 15 (1983).
14. E. BECK AND S. KEMMLER-SACK, *J. Less-Common Met.* **135,** 257 (1987).
15. A. W. SLEIGHT AND R. J. BOUCHARD, "National Bureau of Standards Special Publication 364: Solid State Chemistry, Proceedings of 5th Materials Research Symposium" (1972).
16. J. B. GOODENOUGH, A. HAMNETT, AND D. TELLES, *in* "Localization and Metal–Insulator Transition" (H. Fritzsche and D. Adler, Eds.), Plenum, New York (1985).
17. F. IZUMI, *J. Mineral. Soc. Japan* **17,** 37 (1985). [in Japanese]
18. R. A. BEYERLEIN, H. S. HOROWITZ, J. M. LONGO, M. E. LEONOWICZ, J. D. JORGENSEN, AND F. J. ROTELLA, *J. Solid State Chem.* **51,** 253 (1984).
19. J. B. GOODENOUGH, J. A. KAFALAS, AND J. M. LONGO, "Preparative Methods in Solid State Chemistry," p. 1, Academic Press, New York (1972).
20. J. E. GREEDAN, *J. Less-Common Met.* **111,** 335 (1985).